Differential Algebraic Equations and Averaged Models for Switched Capacitor Converters with State Jumps

Elisa Mostacciuolo, Francesco Vasca, *Senior Member, IEEE*, and Silvio Baccari

***Abstract*—Switched capacitor converters with ideal switches exhibit discontinuities in the electrical variables, i.e., state jumps at the switching time instants. This feature introduces some difficulties for the determination of compact dynamic models for these power converters. In this paper, we tackle the issue by considering a switched model where the dynamics of the modes are represented through differential algebraic equations. For this class of systems the classical averaged model fails. By including a suitable jump mode that approximates the state discontinuities, a generalized frequency-dependent averaged model is proposed. The effectiveness of the switched and averaged models is numerically and experimentally verified by analyzing the ladder, series–parallel, Fibonacci, and Dickson topologies, and by considering different switching frequencies, voltage sources, and circuits parameters.**

***Index Terms*—Differential equations, DC-DC power conversion, frequency domain analysis, ladder circuits, modeling, power converter, switched capacitor circuits, switched systems, time domain analysis.**

I. Introduction

SWITCHED capacitor (SC) converters have recently gained an increasing interest due to their advantages for many applications [1], [2]. The dynamic behavior of these converters is nontrivial to be modeled. The ideal switches behavior determines state discontinuities, so called state jumps, which prevent the use of classical switched and averaged models [3]. In the presence of state jumps, the representation of the converter modes by means of ordinary differential equations (ODE) must be combined with algebraic constraints depending on the active mode [4]. Various techniques have been presented in the literature in order to address this issue. A discrete-time framework for the analysis of SC converters has been proposed in [5]. In [6], the constraints on the electrical variables for the different modes are obtained by referring to the charge balance principle. A steady-state energy-flow-path approach has been used in [7] for the investigation of the efficiency in complex SC converters. In this paper, we consider the analysis of the converters by means of switched differential algebraic equations (SDAE). This framework has been widely used for systems with state jumps [8] and has been proposed in [9] for fault detection of power converters. As a first contribution of this paper, we present the SDAE models for several topologies of SC converters. The proposed model allows to naturally capture the switching behavior and the state jumps without requiring modes-dependent algebraic manipulations.

Usually, the nonsmoothness of switched models of power converters is considered as a problem for their analysis and control design. A typical approach in order to overcome this issue consists of averaging the switched dynamics over a time interval [10]. Unfortunately, classical averaged models fail in the presence of state jumps and a straightforward extension of the averaging technique from switched ODE to SDAE is nontrivial. An averaged model for homogeneous SDAE systems with two modes is proposed in [11]. This result is extended to the case of multimode SDAE in [12], [13], whereas an averaging result for the case of non homogeneous SDAE is presented in [14]. The averaged models of SDAE proposed in the existing literature require some technical assumptions that are not satisfied for typical SC converters such as ladder, series–parallel, Fibonacci, and Dickson topologies. On the other hand the time evolution of the state of these circuits clearly show a sort of averaged dynamics. The averaged model proposed in this paper is based on the preliminary idea presented by Mostacciuolo and Vasca in [15]. Herein the formulation of the averaged model is formally fixed by adding a jump mode that takes into account for the presence of state jumps. A procedure for the design of the jump modes parameters is also discussed. By applying the averaging technique to the resulting switched system, an averaged model with frequency-dependent dynamic matrix is obtained.

The paper is organized as follows. In Section II some preliminaries and a brief reminder on the required theory of SDAE are presented. The SDAE models of the ladder, series–parallel, Fibonacci, and Dickson SC converters are presented in Section III. Section IV illustrates the idea and the structure of the proposed averaged model. The numerical and experimental results analyzed in Sections V and VI, respectively, demonstrate the effectiveness of our switched and averaged models. The conclusions are presented in Section VII.

II. Preliminaries on Switched DAEs

In this section, some preliminaries and notions on the SDAE models of interest are presented. A linear continuous-time DAE

Manuscript received January 17, 2017; revised March 23, 2017; accepted April 24, 2017. Date of publication May 9, 2017; date of current version January 3, 2018. Recommended for publication by Associate Editor C. K. Tse. *(Corresponding author: Elisa Mostacciuolo.)*

The authors are with the Department of Engineering, University of Sannio, Benevento 82100, Italy (e-mail: elisa.mostacciuolo@unisannio.it; vasca@unisannio.it; baccari@unisannio.it).

Color versions of one or more of the figures in this paper are available online at http://ieeexplore.ieee.org.

Digital Object Identifier 10.1109/TPEL.2017.2702389

can be written as

$$E\dot{x}(t) = Ax(t) + Bu(t) \tag{1}$$

where $t \in \mathbb{R}_+$ is the time, $x \in \mathbb{R}^n$ is the state, $u(t) : \mathbb{R}_+ \to \mathbb{R}^m$ is the input, which is assumed to be Lipschitz continuous, $x(0^-) = x_0$ is the initial condition, and $E \in \mathbb{R}^{n\times n}$, $A \in \mathbb{R}^{n\times n}$, $B \in \mathbb{R}^{n\times m}$ are constant matrices. In general, the matrix E is singular and then the representation (1) includes some algebraic constraints that involve state variables and inputs.

A matrix pair (E, A) is *regular* if and only if the polynomial $\det(sE - A)$ is not the zero polynomial for any complex variable s. For any regular matrix pair (E, A) there exist transformation matrices $S \in \mathbb{R}^{n\times n}$, $T \in \mathbb{R}^{n\times n}$ that put (E, A) into the quasi-Weierstrass form

$$(\mathrm{SET}, \mathrm{SAT}) = \left(\begin{bmatrix} I & 0 \\ 0 & N \end{bmatrix}, \begin{bmatrix} J & 0 \\ 0 & I \end{bmatrix} \right) \tag{2}$$

where $N \in \mathbb{R}^{n_2\times n_2}$, with $0 \le n_2 \le n$, is a nilpotent matrix, $J \in \mathbb{R}^{n_1\times n_1}$, with $n_1 = n - n_2$, is some matrix and I is the identity matrix of the appropriate size. The transformation matrices are given by

$$T = [V,\ W], \quad S = [EV,\ AW]^{-1} \tag{3}$$

where the matrices $V \in \mathbb{R}^{n\times n_1}$ and $W \in \mathbb{R}^{n\times n_2}$ can be obtained by implementing algorithms based on the Wong sequences so as detailed in Algorithm 2.

The knowledge of the transformation matrices S and T, allows one to define the following mathematical operators that play a key role in the solution of a DAE. Consider a regular matrix pair (E, A) and its quasi-Weierstrass form (2). The *consistency projector* Π, the *differential projector* Π^{diff}, and the *impulsive projector* Π^{imp} of (E, A) are defined as

$$\Pi = T \begin{bmatrix} I & 0 \\ 0 & 0 \end{bmatrix} T^{-1},\ \Pi^{\mathrm{diff}} = T \begin{bmatrix} I & 0 \\ 0 & 0 \end{bmatrix} S,\ \Pi^{\mathrm{imp}} = T \begin{bmatrix} 0 & 0 \\ 0 & I \end{bmatrix} S \tag{4}$$

respectively. Differently from the impulsive and differential, the consistency projector is an idempotent matrix, i.e., $\Pi^2 = \Pi$. The *flow matrix* A^{diff} of a regular matrix pair (E, A) is defined as

$$A^{\mathrm{diff}} = T \begin{bmatrix} J & 0 \\ 0 & 0 \end{bmatrix} T^{-1}. \tag{5}$$

By using (4) and (2) it follows:

$$\Pi^{\mathrm{diff}} A = T \begin{bmatrix} I & 0 \\ 0 & 0 \end{bmatrix} SA = T \begin{bmatrix} I & 0 \\ 0 & 0 \end{bmatrix} \begin{bmatrix} J & 0 \\ 0 & I \end{bmatrix} T^{-1} = A^{\mathrm{diff}}. \tag{6}$$

Moreover it is easy to verify that $A^{\mathrm{diff}}\Pi = A^{\mathrm{diff}} = \Pi A^{\mathrm{diff}}$.

An initial condition $x(0^-)$ is *consistent* if satisfies at $t = 0$ the algebraic constraints in (1). For any regular matrix pairs (E, A) each solution of (1) is uniquely determined by any consistent initial condition. If $x(0^-)$ is not consistent, jumps and impulses in the state can occur. Sufficient conditions to guarantee the absence of impulses in the solution of (1) with a regular matrix pair (E, A) are [16]

$$\Pi^{\mathrm{imp}} E = 0, \quad \Pi^{\mathrm{imp}} B = 0. \tag{7}$$

In this case, the solution formula of (1) is given by [8]

$$x(t) = e^{A^{\mathrm{diff}} t}\Pi x(0^-) + \int_0^t e^{A^{\mathrm{diff}}(t-\tau)}\Pi^{\mathrm{diff}} B u(\tau) d\tau \tag{8}$$

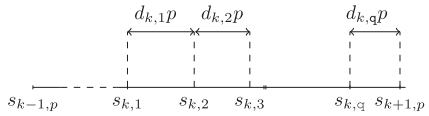

Fig. 1. Graphical representation of the time interval $[kp, (k+1)p]$, with $s_{k,i} := kp + \sum_{j=1}^{i-1} d_{k,j}p\ i = 1, \ldots, \mathtt{q}$.

where the state jump at the initial time instant is determined by the consistency projector, i.e., $x(0^+) = \Pi x(0^-)$.

An SDAE can be written as

$$E_{\sigma(t)}\dot{x}(t) = A_{\sigma(t)}x(t) + B_{\sigma(t)}u(t) \tag{9}$$

where the switching signal $\sigma(t) : \mathbb{R}_+ \to \Sigma$ is assumed to be a piece-wise constant right-continuous function, that selects at each time instant the index $i \in \Sigma := \{1, \ldots, \mathtt{q}\}$ of the active mode, where $\mathtt{q}$ is the finite number of modes. The dynamics of each mode of (9) is described by a linear DAE in the form (1) with matrices $E_i \in \mathbb{R}^{n\times n}$, $A_i \in \mathbb{R}^{n\times n}$, and $B_i \in \mathbb{R}^{n\times m}$, where without loss of generality, we assume the same numbers of state variables and inputs for all modes. The sequence of modes considered in this paper repeats with a constant time interval $p > 0$, say the switching period. The switching time instants are defined as

$$s_{k,i} := kp + \sum_{j=1}^{i-1} d_{k,j}p \tag{10}$$

where $i \in \Sigma$, k is a nonnegative integer that identifies the kth switching period and $d_{k,j} \in (0, 1)$ is the duty cycle of the jth mode in the kth switching period, see Fig. 1; in particular, $\sum_{j=1}^{\mathtt{q}} d_{k,j} = 1$ for all k. Then the switching signal can be written as

$$\sigma(t) = \begin{cases} 1, & t \in [s_{k,1}, s_{k,2}) \\ 2, & t \in [s_{k,2}, s_{k,3}) \\ \vdots & \\ \mathtt{q}, & t \in [s_{k,\mathtt{q}}, s_{k+1,1}) \end{cases} \tag{11}$$

for $t \in [kp, (k+1)p)$ and $k = 0, 1, \ldots$. The dynamics of the ith mode, $i \in \Sigma$, are given by a linear DAE, whose solution evolves within a consistency space. The consistency spaces corresponding to the different modes do not need to coincide, i.e., the value $x(s_{k,i}^-)$ at the switching time instant $s_{k,i}$ which concludes the $(i-1)$th mode is not necessarily in the consistency space of the starting ith mode. Each consistency projector Π_i projects the state $x(s_{k,i}^-)$ in the space of consistency relative to the ith mode. In the following we assume that the conditions of absence of impulses (7) hold for all modes

$$\Pi_i^{\mathrm{imp}} E_i = 0 \tag{12a}$$

$$\Pi_i^{\mathrm{imp}} B_i^{\mathrm{diff}} = 0 \tag{12b}$$

for all $i \in \Sigma$, where $B_i^{\mathrm{diff}} = \Pi_i^{\mathrm{diff}} B_i$ and the projectors of the different modes are defined according to (4). Then from the regularity of the pairs (E_i, A_i) and the repetitive use of (8), it is possible to represent the SDAE system (9) in terms of the

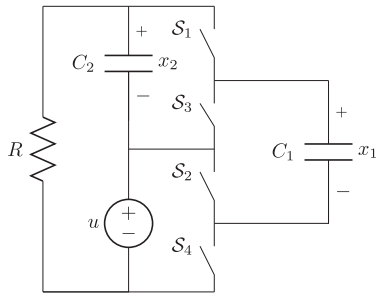

Fig. 2. Ladder converter topology with ideal switches.

following equivalent switched ODE with jumps

$$\dot{x}(t) = A_i^{\text{diff}} x(t) + B_i^{\text{diff}} u(t) \tag{13a}$$

$$x(s_{k,i}^+) = \Pi_i x(s_{k,i}^-) \tag{13b}$$

where $x(s_{0,1}^-) = x(0^-)$, $t \in (s_{k,i}, s_{k,i+1})$, $i \in \Sigma$, k is a nonnegative integer, and A_i^{diff} is given by (5) applied to the specific ith mode. Further details on the SDAE theory can be found in [8].

III. SDAE for SC Converters

In this section we present the SDAE model for the ladder, series–parallel, Fibonacci, and Dickson SC converters. Details on the converters topologies can be found in [17], [18]. The switches are assumed to be ideal and are denoted by $\mathcal{S}_z$ with $z = 1, \ldots, \bar{z}$ being the index for the different switches. For the sake of clarity we present the models by considering the DAE representation of each mode.

A. Ladder Converter

A typical elementary cell of a ladder step-up SC converter is shown in Fig. 2. The circuit consists of two capacitors and four switches ($\bar{z} = 4$) that are controlled in a complementary way. In the first mode ($\sigma = 1$) the switches $\mathcal{S}_z$ with $z = \{1, 2\}$ are ON and those with $z = \{3, 4\}$ are OFF. Then the capacitors C_1 and C_2 are in parallel and the mode is described by the following set of equations:

$$RC_1\dot{x}_1(t) + RC_2\dot{x}_2(t) = -x_2(t) - u(t) \tag{14a}$$

$$0 = x_1(t) - x_2(t) \tag{14b}$$

where x_1 and x_2 are the voltages on the capacitors C_1 and C_2, respectively. The second mode ($\sigma = 2$) corresponds to the complementary switches states, i.e., $\mathcal{S}_z$ is OFF for $z = \{1, 2\}$ and ON for $z = \{3, 4\}$. In this mode the circuit equations become

$$RC_2\dot{x}_2(t) = -x_2(t) - u(t) \tag{15a}$$

$$0 = -x_1(t) + u(t). \tag{15b}$$

By considering (14) and (15), and by computing the matrices Π_2^{imp} and B_2 it is easy to verify that (12b) for $\sigma = 2$ does not hold. As an alternative we can lightly restrict the class of inputs of interest and include an input signal model into the state equations. For instance by considering as input a constant voltage source $u(t) = \bar{u}$, for $t \in \mathbb{R}_+$ we can describe the circuit by adding a dummy state variable, say x_3, such that $\dot{x}_3(t) = 0$ and $x_3(0) = \bar{u}$. Then the matrices pairs of the two modes become

$$E_1 = \begin{bmatrix} RC_1 & RC_2 & 0 \\ 0 & 0 & 0 \\ 0 & 0 & 1 \end{bmatrix}, \quad A_1 = \begin{bmatrix} 0 & -1 & -1 \\ 1 & -1 & 0 \\ 0 & 0 & 0 \end{bmatrix}$$

$$E_2 = \begin{bmatrix} 0 & RC_2 & 0 \\ 0 & 0 & 0 \\ 0 & 0 & 1 \end{bmatrix}, \quad A_2 = \begin{bmatrix} 0 & -1 & -1 \\ -1 & 0 & 1 \\ 0 & 0 & 0 \end{bmatrix}. \tag{16}$$

From (16) and by applying the procedure in Algorithm 2 we obtain

$$V_1 = \begin{bmatrix} 1 & 0 \\ 1 & 0 \\ 0 & 1 \end{bmatrix}, W_1 = \begin{bmatrix} 1 \\ -\dfrac{C_1}{C_2} \\ 0 \end{bmatrix}, V_2 = \begin{bmatrix} 1 & 0 \\ 0 & 1 \\ 1 & 0 \end{bmatrix}, W_2 = \begin{bmatrix} 1 \\ 0 \\ 0 \end{bmatrix}. \tag{17}$$

By using (16) and (17) in (3) one obtains the transformation matrices

$$S_1 = \begin{bmatrix} \dfrac{1}{R(C_1+C_2)} & \dfrac{-C_1}{R(C_1+C_2)^2} & 0 \\ 0 & 0 & 1 \\ 0 & \dfrac{C_2}{(C_1+C_2)} & 0 \end{bmatrix}$$

$$S_2 = \begin{bmatrix} 0 & 0 & 1 \\ \dfrac{1}{RC_2} & 0 & 0 \\ 0 & -1 & 0 \end{bmatrix}$$

$$T_1 = \begin{bmatrix} 1 & 0 & 1 \\ 1 & 0 & -\dfrac{C_1}{C_2} \\ 0 & 1 & 0 \end{bmatrix}, \quad T_2 = \begin{bmatrix} 1 & 0 & 1 \\ 0 & 1 & 0 \\ 1 & 0 & 0 \end{bmatrix}. \tag{18}$$

Then from (4) and (5) the consistency projectors and the corresponding flow matrices are given by

$$\Pi_1 = \frac{1}{C_1+C_2}\begin{bmatrix} C_1 & C_2 & 0 \\ C_1 & C_2 & 0 \\ 0 & 0 & C_1+C_2 \end{bmatrix}, \Pi_2 = \begin{bmatrix} 0 & 0 & 1 \\ 0 & 1 & 0 \\ 0 & 0 & 1 \end{bmatrix}$$

$$A_1^{\text{diff}} = \frac{1}{R(C_1+C_2)^2}\begin{bmatrix} -C_1 & -C_2 & -(C_1+C_2) \\ -C_1 & -C_2 & -(C_1+C_2) \\ 0 & 0 & 0 \end{bmatrix}$$

$$A_2^{\text{diff}} = \frac{1}{RC_2}\begin{bmatrix} 0 & 0 & 0 \\ 0 & -1 & -1 \\ 0 & 0 & 0 \end{bmatrix}. \tag{19}$$

With this reformulation it is easy to verify that (12) hold.

B. Series–Parallel Converter

The series–parallel topology of a step-down SC power converter is shown in Fig. 3. The seven switches of the circuit are driven in a complementary way. During the first mode the switches $\mathcal{S}_z$ with $z = \{1, 2, 5, 6\}$ are ON, and those with $z = \{3, 4, 7\}$ are OFF. Then the two capacitors C_1, C_2 are in parallel. In the second mode the switches with $z = \{1, 2, 5, 6\}$ are OFF and the others are ON, thus, the two capacitors are

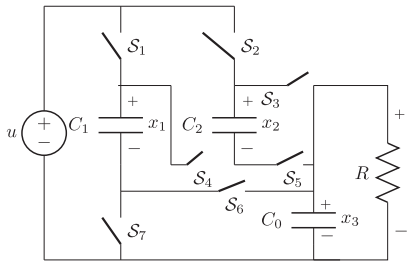

Fig. 3. Series–parallel topology with ideal switches.

in series. In the first mode, the input influences the algebraic constraints, i.e., $x_1(t) + x_3(t) = u(t)$ and (12b) does not hold. We then introduce a new state variable, say x_4, in order to model the constant source $u(t) = \bar{u}$ for $t \in \mathbb{R}_+$, i.e., $\dot{x}_4(t) = 0$, $x_4(0) = \bar{u}$. The corresponding SDAE (9) is defined by the matrices

$$E_1 = \begin{bmatrix} C_1 & C_2 & -C_0 & 0 \\ 0 & 0 & 0 & 0 \\ 0 & 0 & 0 & 0 \\ 0 & 0 & 0 & 1 \end{bmatrix}, \quad A_1 = \begin{bmatrix} 0 & 0 & \frac{1}{R} & 0 \\ 1 & 0 & 1 & -1 \\ 1 & -1 & 0 & 0 \\ 0 & 0 & 0 & 0 \end{bmatrix}$$

$$E_2 = \begin{bmatrix} C_1 & -C_2 & 0 & 0 \\ 0 & C_2 & C_0 & 0 \\ 0 & 0 & 0 & 0 \\ 0 & 0 & 0 & 1 \end{bmatrix}, \quad A_2 = \begin{bmatrix} 0 & 0 & 0 & 0 \\ 0 & 0 & -\frac{1}{R} & 0 \\ 1 & 1 & -1 & 0 \\ 0 & 0 & 0 & 0 \end{bmatrix}. \tag{20}$$

By considering the Wong sequences we can compute the corresponding V_i and W_i, $i = 1, 2$

$$V_1 = \begin{bmatrix} 1 & 0 \\ 1 & 0 \\ 0 & 1 \\ 1 & 1 \end{bmatrix}, \quad W_1 = \begin{bmatrix} 1 & 0 \\ 0 & 1 \\ \frac{C_1}{C_0} & \frac{C_2}{C_0} \\ 0 & 0 \end{bmatrix}$$

$$V_2 = \begin{bmatrix} 1 & 0 & 0 \\ 0 & 1 & 0 \\ 1 & 1 & 0 \\ 0 & 0 & 1 \end{bmatrix}, \quad W_2 = \begin{bmatrix} 1 \\ \frac{C_1}{C_2} \\ -\frac{C_1}{C_0} \\ 0 \end{bmatrix}. \tag{21}$$

From (21) it is straightforward to obtain the consistency projectors by using (4), the flow matrices through (5), and to verify that (12) hold.

C. Fibonacci Converter

An equivalent scheme of the Fibonacci SC topology is shown in Fig. 4. The following two modes are considered: $\sigma = 1$ corresponds to $\mathcal{S}_z$ being ON for $z = \{1, 3, 6, 8, 10\}$ and OFF for $z = \{2, 4, 5, 7, 9\}$, whereas $\sigma = 2$ is characterized by the complementary conducting states of the switches. The matrices pairs (E_i, A_i), $i = 1, 2$ corresponding to these modes of the circuit

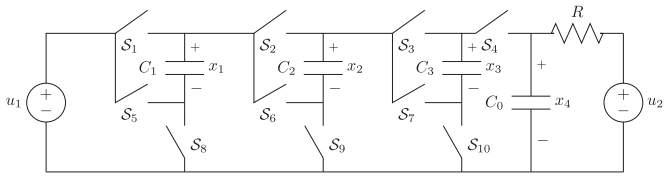

Fig. 4. Fibonacci topology with ideal switches.

are given by

$$E_1 = \begin{bmatrix} 0 & C_2 & C_3 & 0 & 0 & 0 \\ 0 & 0 & 0 & C_0 & 0 & 0 \\ 0 & 0 & 0 & 0 & 0 & 0 \\ 0 & 0 & 0 & 0 & 0 & 0 \\ 0 & 0 & 0 & 0 & 1 & 0 \\ 0 & 0 & 0 & 0 & 0 & 1 \end{bmatrix}$$

$$A_1 = \begin{bmatrix} 0 & 0 & 0 & 0 & 0 & 0 \\ 0 & 0 & 0 & -\frac{1}{R} & 0 & \frac{1}{R} \\ 1 & 1 & -1 & 0 & 0 & 0 \\ 1 & 0 & 0 & 0 & -1 & 0 \\ 0 & 0 & 0 & 0 & 0 & 0 \\ 0 & 0 & 0 & 0 & 0 & 0 \end{bmatrix}$$

$$E_2 = \begin{bmatrix} C_1 & C_2 & -C_3 & 0 & 0 & 0 \\ 0 & 0 & C_3 & C_0 & 0 & 0 \\ 0 & 0 & 0 & 0 & 0 & 0 \\ 0 & 0 & 0 & 0 & 0 & 0 \\ 0 & 0 & 0 & 0 & 1 & 0 \\ 0 & 0 & 0 & 0 & 0 & 1 \end{bmatrix}$$

$$A_2 = \begin{bmatrix} 0 & 0 & 0 & 0 & 0 & 0 \\ 0 & 0 & 0 & -\frac{1}{R} & 0 & \frac{1}{R} \\ 1 & -1 & 0 & 0 & 1 & 0 \\ 0 & 1 & 1 & -1 & 0 & 0 \\ 0 & 0 & 0 & 0 & 0 & 0 \\ 0 & 0 & 0 & 0 & 0 & 0 \end{bmatrix}. \tag{22}$$

Note that the state variables x_5 and x_6 have been introduced in order to represent the two constant sources $u_1(t) = \bar{u}_1$ and $u_2(t) = \bar{u}_2$ for $t \in \mathbb{R}_+$, respectively. The matrices V_i and W_i, $i = 1, 2$, obtained by applying the procedure described in Algorithm 2, are

$$V_1 = \begin{bmatrix} 1 & 0 & 0 & 0 \\ 0 & 1 & 0 & 0 \\ 1 & 1 & 0 & 0 \\ 0 & 0 & 1 & 0 \\ 1 & 0 & 0 & 0 \\ 0 & 0 & 0 & 1 \end{bmatrix}, \quad W_1 = \begin{bmatrix} 1 & 0 \\ 0 & 1 \\ 0 & -C_2/C_3 \\ 0 & 0 \\ 0 & 0 \\ 0 & 0 \end{bmatrix}$$

$$V_2 = \begin{bmatrix} 1 & 0 & 0 & 0 \\ 0 & 1 & 0 & 0 \\ 0 & 0 & 1 & 0 \\ 0 & 1 & 1 & 0 \\ -1 & 1 & 0 & 0 \\ 0 & 0 & 0 & 1 \end{bmatrix}, \quad W_2 = \begin{bmatrix} 1 & 0 \\ 0 & 1 \\ C_1/C_3 & C_2/C_3 \\ -C_1/C_0 & -C_2/C_0 \\ 0 & 0 \\ 0 & 0 \end{bmatrix}. \tag{23}$$

Hence from (23) it is easy to compute the projectors and the flow matrices of the two modes according to (4) and (5), respectively.

The SDAE homogeneous model can be derived also for other inputs of interest, such as sinusoidal signals. To this aim let us assume

$$u_1(t) = \bar{u}_1 + U\sin(\omega t), \quad u_2(t) = \bar{u}_2 \tag{24}$$

with ω and U the frequency and the amplitude of the sinusoidal input, respectively. In order to include the sinusoidal source $u_1(t)$ into the homogeneous state equations, we introduce two further dummy state variables, say x_7 and x_8, whose dynamic equations are given by

$$\dot{x}_7(t) = -\omega x_8(t), \quad \dot{x}_8(t) = \omega x_7(t) \tag{25}$$

with $x_7(0) = 0$ and $x_8(0) = 1$. Therefore, one can write $u_1(t) = x_5(t) + Ux_7(t)$ and the matrices of the two modes become

$$E_1 = \begin{bmatrix} 0 & C_2 & C_3 & 0 & 0 & 0 & 0 & 0 \\ 0 & 0 & 0 & C_0 & 0 & 0 & 0 & 0 \\ 0 & 0 & 0 & 0 & 0 & 0 & 0 & 0 \\ 0 & 0 & 0 & 0 & 0 & 0 & 0 & 0 \\ 0 & 0 & 0 & 0 & 1 & 0 & 0 & 0 \\ 0 & 0 & 0 & 0 & 0 & 1 & 0 & 0 \\ 0 & 0 & 0 & 0 & 0 & 0 & 1 & 0 \\ 0 & 0 & 0 & 0 & 0 & 0 & 0 & 1 \end{bmatrix}$$

$$A_1 = \begin{bmatrix} 0 & 0 & 0 & 0 & 0 & 0 & 0 & 0 \\ 0 & 0 & 0 & -\frac{1}{R} & 0 & \frac{1}{R} & 0 & 0 \\ 1 & 1 & -1 & 0 & 0 & 0 & 0 & 0 \\ -1 & 0 & 0 & 0 & 1 & 0 & U & 0 \\ 0 & 0 & 0 & 0 & 0 & 0 & 0 & 0 \\ 0 & 0 & 0 & 0 & 0 & 0 & 0 & 0 \\ 0 & 0 & 0 & 0 & 0 & 0 & 0 & -\omega \\ 0 & 0 & 0 & 0 & 0 & 0 & \omega & 0 \end{bmatrix}$$

$$E_2 = \begin{bmatrix} C_1 & C_2 & -C_3 & 0 & 0 & 0 & 0 & 0 \\ 0 & 0 & C_3 & C_0 & 0 & 0 & 0 & 0 \\ 0 & 0 & 0 & 0 & 0 & 0 & 0 & 0 \\ 0 & 0 & 0 & 0 & 0 & 0 & 0 & 0 \\ 0 & 0 & 0 & 0 & 1 & 0 & 0 & 0 \\ 0 & 0 & 0 & 0 & 0 & 1 & 0 & 0 \\ 0 & 0 & 0 & 0 & 0 & 0 & 1 & 0 \\ 0 & 0 & 0 & 0 & 0 & 0 & 0 & 1 \end{bmatrix}$$

$$A_2 = \begin{bmatrix} 0 & 0 & 0 & 0 & 0 & 0 & 0 & 0 \\ 0 & 0 & 0 & -\frac{1}{R} & 0 & \frac{1}{R} & 0 & 0 \\ 1 & -1 & 0 & 0 & 1 & 0 & U & 0 \\ 0 & 1 & 1 & -1 & 0 & 0 & 0 & 0 \\ 0 & 0 & 0 & 0 & 0 & 0 & 0 & 0 \\ 0 & 0 & 0 & 0 & 0 & 0 & 0 & 0 \\ 0 & 0 & 0 & 0 & 0 & 0 & 0 & -\omega \\ 0 & 0 & 0 & 0 & 0 & 0 & \omega & 0 \end{bmatrix} \tag{26}$$

from which the corresponding flow matrices and projectors can be easily obtained.

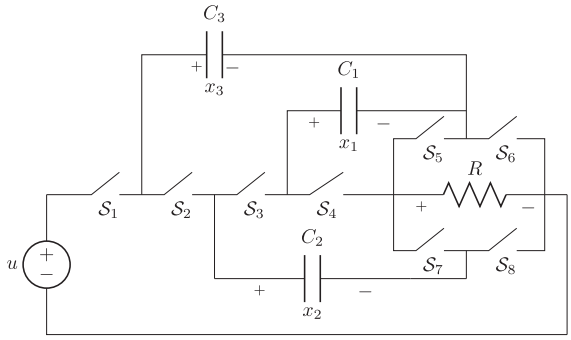

Fig. 5. Dickson SC converter with ideal switches.

D. Dickson Converter

Let us consider the 4:1 Dickson SC converter shown in Fig. 5. The switches are controlled such that in the first mode we have $\mathcal{S}_z$ being ON for $z = \{1, 3, 5, 8\}$ and OFF for $z = \{2, 4, 6, 7\}$, and viceversa for the second mode. The matrices pairs of the two modes are

$$E_1 = \begin{bmatrix} C_1 & C_2 & 0 & 0 \\ -RC_1 & 0 & -RC_3 & 0 \\ 0 & 0 & 0 & 0 \\ 0 & 0 & 0 & 1 \end{bmatrix}, \; A_1 = \begin{bmatrix} 0 & 0 & 0 & 0 \\ 1 & -1 & 0 & 0 \\ -1 & 1 & 1 & -1 \\ 0 & 0 & 0 & 0 \end{bmatrix}$$

$$E_2 = \begin{bmatrix} 0 & C_2 & C_3 & 0 \\ -RC_1 & RC_2 & 0 & 0 \\ 0 & 0 & 0 & 0 \\ 0 & 0 & 0 & 1 \end{bmatrix}, \; A_2 = \begin{bmatrix} 0 & 0 & 0 & 0 \\ 1 & 0 & 0 & 0 \\ 1 & 1 & -1 & 0 \\ 0 & 0 & 0 & 0 \end{bmatrix} \tag{27}$$

where the fourth state variable is used to represent the constant source $u(t) = \bar{u}$ for $t \in \mathbb{R}_+$. The transformation matrices obtained by using the Wong sequences are given by

$$V_1 = \begin{bmatrix} 1 & 0 & 0 \\ 0 & 1 & 0 \\ 0 & 0 & 1 \\ -1 & 1 & 1 \end{bmatrix}, \quad W_1 = \begin{bmatrix} 1 \\ -\frac{C_1}{C_2} \\ -\frac{C_2}{C_3} \\ 0 \end{bmatrix}$$

$$V_2 = \begin{bmatrix} 1 & 0 & 0 \\ 0 & 1 & 0 \\ 1 & 1 & 0 \\ 0 & 0 & 1 \end{bmatrix}, \quad W_2 = \begin{bmatrix} 1 \\ \frac{C_1}{C_2} \\ -\frac{C_1}{C_3} \\ 0 \end{bmatrix}. \tag{28}$$

From (28) and by considering (4) and (5), one obtains the corresponding projectors and flow matrices.

IV. Frequency-Dependent Averaged Model

The SDAE models of the power converters analyzed in the previous section can be represented, for that specific inputs, in

the following form

$$E_{\sigma(t)}\dot{x}(t) = A_{\sigma(t)}x(t) \tag{29}$$

i.e., (9) with $u(t) = 0$, with the switching signal $\sigma(t)$ defined by (10) and (11). For this class of homogeneous SDAE, the following assumptions are used in [19] to provide an averaging results

$$\operatorname{im}\Pi_{\cap} \subseteq \operatorname{im}\Pi_i, \quad \ker\Pi_{\cap} \supseteq \ker\Pi_i \tag{30}$$

for all $i \in \Sigma$, with $\Pi_{\cap} = \Pi_{\mathsf{q}} \cdots \Pi_1$. It is easy to verify that (30) do not hold for the power converters considered above. On the other hand the time evolution of the states of SC converters show an averaged dynamic behavior also under lossless operating conditions [20].

A. Averaged Model for SDAE

The proposed averaged model is obtained by adding after each switching time instant a jump mode. In order to represent the rational behind our model construction, let us consider the state at the end of a generic $(i-1)$th mode, say x_{i-1}^-. When the ith mode starts, a jump may occur resetting the state at $\Pi_i x_{i-1}^-$. The dynamic matrix of the ith jump mode, say $A_{\text{jump},i}$, and the corresponding duration of the jump mode, say $\Delta_i p$, are chosen such that at the end of that mode the state $x(s_{k_i} + \Delta_i p)$ approximates $\Pi_i x_{i-1}^-$. The dynamics of the jump mode is represented with the following ODE

$$\dot{x}(t) = A_{\text{jump},i}x(t) \tag{31}$$

and the corresponding solution can be written as

$$x(t) = e^{A_{\text{jump},i}(t-s_{k,i})}x_{i-1}^- \tag{32}$$

for $t \in [s_{k,i}, s_{k,i} + \Delta_i p]$. By using the Taylor series of the matrix exponential one can write

$$x(s_{k,i} + \Delta_i p) = e^{A_{\text{jump},i}\Delta_i p}x_{i-1}^- = \sum_{h=0}^{\infty} \frac{(A_{\text{jump},i}\Delta_i p)^h}{h!}x_{i-1}^-. \tag{33}$$

The dynamic matrix is chosen as

$$A_{\text{jump},i} := \begin{cases} -(I-\Pi_i)\frac{\log((\alpha p)^{-1})}{\Delta_i p} & \text{if } \Delta_i \neq 0 \\ 0 & \text{if } \Delta_i = 0 \end{cases} \tag{34}$$

where $\alpha \in \mathbb{R}_+$ is a parameter to be selected and the duty cycle Δ_i is given by

$$\Delta_i = \Delta\|\Pi_i - I\|. \tag{35}$$

The parameter Δ is selected such that $\Delta_i \ll d_{k,i}$ for all k, i. To this purpose we define Δ by taking into account the minimum value of the duty cycles and the maximum norm of the difference between the identity matrix and the consistency projectors

$$\Delta = \epsilon\frac{d_{\min}}{\mu} \tag{36}$$

where $\epsilon \ll 1$ is a parameter to be chosen, $d_{\min} = \min_{i\in\Sigma,k\in\mathbb{N}} d_{k,i}$ is the minimum duty cycle and $\mu = \max\{1, \max_{i\in\Sigma}\|\Pi_i - I\|\}$. By substituting (34) in (33) one obtains

$$\begin{aligned} x(s_{k,i} + \Delta_i p) &= \sum_{h=0}^{\infty} \frac{(\Pi_i - I)^h \log((\alpha p)^{-1})^h}{h!}x_{i-1}^- \\ &= x_{i-1}^- + \sum_{h=1}^{\infty} \frac{(\Pi_i - I)^h \log((\alpha p)^{-1})^h}{h!}x_{i-1}^- \\ &\hat{=} \Pi_i x_{i-1}^- + (I-\Pi_i)\sum_{h=0}^{\infty} \frac{(-\log((\alpha p)^{-1}))^h}{h!}x_{i-1}^- \\ &= \Pi_i x_{i-1}^- + (I-\Pi_i)e^{-\log((\alpha p)^{-1})}x_{i-1}^- \\ &= \Pi_i x_{i-1}^- + (I-\Pi_i)\alpha p x_{i-1}^- \end{aligned} \tag{37}$$

where in " $\hat{=}$ " is used the relation

$$(\Pi_i - I)^h = (-1)^h(I - \Pi_i) \tag{38}$$

for any positive integer h, which follows from the idempotence property of the consistency projectors and for " $\hat{=}$ " it is assumed $\alpha p < 1$. By choosing α such that $\alpha p \ll 1$ one should expect that the state at the end of the "fast" jump mode approximates the state discontinuity occurring in the SDAE of the switching time instant. This conjecture will be verified in the next sections through numerical and experimental results.

Taking into account all jump modes, the SDAE (29) is approximated with the following switched ODE model

$$\dot{x}(t) = \begin{cases} A_{\text{jump},i}\ x(t), & t \in [s_{k,i}, s_{k,i} + \Delta_i p) \\ A_i^{\text{diff}}\ \ x(t), & t \in [s_{k,i} + \Delta_i p, s_{k,i+1}) \end{cases} \tag{39}$$

for $t \in [s_{k,i}, s_{k,i+1})$, $i \in \Sigma$ representing the active mode according to (10)–(11), k the nonnegative integer representing the current switching period and $x(0^-)$ the initial condition. The proposed averaged model with solution x_{av}, is obtained by taking the convex hull of the dynamic matrices in (39) over the switching periods, which result in

$$\dot{x}_{\text{av}}(t) = A_{\text{av}}(p, \{d_{k,i}\}_{i=1}^{\mathsf{q}})x_{\text{av}}(t) \tag{40}$$

for $t \in \mathbb{R}_+$ where

$$A_{\text{av}}(p, \{d_{k,i}\}_{i=1}^{\mathsf{q}}) := \sum_{i=1}^{\mathsf{q}} A_i^{\text{diff}}(d_{k,i} - \Delta_i) + A_{\text{jump},i}(p)\Delta_i \tag{41}$$

with A_i^{diff} given by (5) applied to the ith mode, $A_{\text{jump},i}$ given by (34) and Δ_i given by (35) and (36). The duration of the ith mode in (41) relative to the kth period has been reduced to $(d_{k,i} - \Delta_i)p$ in order to preserve the same period p for the total duration of all modes. Note that the averaged matrix (41) becomes time invariant for constant duty cycles.

The model (40) and (41) represents an extension of the classical averaged model. Indeed, if all modes do not present state jumps, then $\Pi_i = I$, which implies that the matrices $A_{\text{jump},i}$ and the parameters Δ_i are all zero, and the classical averaged model is recovered.

Algorithm 1: Averaged model of a regular SDAE.

Data: $\{A_i, E_i, B_i\}_{i=1}^{\mathtt{q}}$, p, $d_{\min}$, ϵ, α
Result: $\{A_i^{\text{diff}}\}_{i=1}^{\mathtt{q}}$, $\{A_{jump,i}\}_{i=1}^{\mathtt{q}}$, $\{B_i^{\text{diff}}\}_{i=1}^{\mathtt{q}}$, $\{\Delta_i\}_{i=1}^{\mathtt{q}}$.
for $i \leftarrow 1$ **to** $\mathtt{q}$ **do**
  /*Projectors for each mode*/
  /*Wong sequences matrices, see Algorithm 2*/
  V_i, $W_i \leftarrow$ getVWspace(E_i, A_i);
  $T_i \leftarrow [V_i,\ W_i]$; $S_i \leftarrow [E_iV_i,\ A_iW_i]^{-1}$;
  Π_i, Π_i^{diff}, $\Pi_i^{\text{imp}} \leftarrow$(4);
end
repeat
  /*Check the impulse free condition for each mode*/
  impulseFreeBCond $\leftarrow$ `verified` (12b);
  $i \leftarrow i + 1$;
until impulseFreeBCond *AND* $i <= \mathtt{q}$;
if *NOT*(impulseFreeBCond) **then**
  /*Fix the input u as the output of a dynamic model*/
  (F, G, $z(0)$): $\dot{z} = Fz$, $u = Gz$;
  /*Expand the state vector*/
  $x \leftarrow [x, z]$;
  for $i \leftarrow 1$ **to** $\mathtt{q}$ **do**
    /*SDAE matrices for the new state vector*/
    $E_i \leftarrow [E_i,\ 0;\ 0,\ I]$;
    $A_i \leftarrow [A_i,\ B_iG;\ 0,\ F]$;
    $B_i \leftarrow 0$;
    /*New projectors for each mode*/
    V_i, $W_i \leftarrow$ getVWspace(E_i, A_i);
    $T_i \leftarrow [V_i,\ W_i]$; $S_i \leftarrow [E_iV_i,\ A_iW_i]^{-1}$;
    Π_i, Π_i^{diff}, $\Pi_i^{\text{imp}} \leftarrow$(4);
  end
end
/*Select the parameter Δ*/
$\mu \leftarrow \max\{1, \max_{i\in\Sigma} \|\Pi_i - I\|\}$;
$\Delta \leftarrow$ (36);
/*Results of the algorithm*/
for $i \leftarrow 1$ **to** $\mathtt{q}$ **do**
  $\Delta_i \leftarrow$(35);
  $A_{\text{jump},i} \leftarrow$(34);
  $A_i^{\text{diff}} \leftarrow$ (6);
  $B_i^{\text{diff}} \leftarrow\ \Pi_i^{\text{diff}} B_i$;
end

Algorithm 2: Function *getVWspace*(E,A).

Data: A, E
Result: V, W
begin
  $[m, n] \leftarrow$ `size`(E);
  /*Computation of V*/
  $V \leftarrow$ `eye`(n, n);
  oldSize $\leftarrow n$; newSize $\leftarrow n$;
  while newSize $=$ oldSize **do**
    /*Basis for the column space of EV, see (44)*/
    basisEV $\leftarrow$ `colspace`(EV);
    /*Preimage of A under basisEV*/
    $H \leftarrow$ `null`([A, basisEV]);
    $V \leftarrow$ `colspace`($H(1:n,:)$)
    oldSize $\leftarrow$ newSize;
    newSize $\leftarrow$ `rank`(V);
  end
  /*Computation of W*/
  $W \leftarrow$ `zeros`($n, 1$);
  oldSize $\leftarrow 0$; newSize $\leftarrow 0$;
  while newSize $=$ oldSize **do**
    /*Basis for the column space of AW, see (45)*/
    basisAW $\leftarrow$ `colspace`(AW);
    /*Preimage of E under basisAW*/
    $H \leftarrow$ `null`([E, basisAW]);
    $W \leftarrow$ `colspace`($H(1:n,:)$);
    oldSize $\leftarrow$ newSize;
    newSize $\leftarrow$ `rank`(W);
  end
end

B. Algorithm for the Derivation of the Averaged Model of a General SDAE

The derivation of the proposed averaged model is summarized in Algorithm 1 that can be applied to any power converter with linear modes and ideal switches. The preliminary step is the representation of each mode by means of a differential algebraic equation in the form (1). The examples presented above show how to do that by considering the different combinations of the switches states. As an alternative, a linear DAE in the form (1) can be derived for each mode starting from the circuit netlist and by using the approach in [21]. The other parameters to be selected in order to run the algorithm are the switching period p, the minimum value of the duty cycles $d_{\min}$, the arbitrary small parameter ϵ in (36), and the value of α which, for instance, can be chosen as $\alpha = 0.1/p$. The algorithm starts with the computation of the projectors (4) for each matrix pair (E_i, A_i). Then the impulse free conditions (12b) are checked. If these conditions hold for all modes, then the matrices of the following averaged model are computed

$$\dot{x}_{\text{av}}(t) = A_{\text{av}}(p, \{d_{k,i}\}_{i=1}^{\mathtt{q}}) x_{\text{av}}(t) + B_{\text{av}}^{\text{diff}}(\{d_{k,i}\}_{i=1}^{\mathtt{q}}) u(t) \tag{42}$$

where $A_{\text{av}}(p, \{d_{k,i}\}_{i=1}^{\mathtt{q}})$ is given by (41) and the input matrix is

$$B_{\text{av}}^{\text{diff}}(\{d_{k,i}\}_{i=1}^{\mathtt{q}}) = \sum_{i=1}^{\mathtt{q}} B_i^{\text{diff}}(d_{k,i} - \Delta_i). \tag{43}$$

If for some mode the condition (12b) is not verified, then the class of inputs is restricted to those representable as the solution of a linear time invariant dynamic model and the state space vector is extended accordingly. Then, so as in the former case, the algorithm concludes with the calculation of the jump mode duration Δ_i and the matrices $A_{\text{jump,i}}$, A_i^{diff}, and B_i^{diff} for each mode.

Note that the impulsive free condition (12a) is not checked in Algorithm 1 because the general solution of a SDAE can be always partitioned into its impulsive and nonimpulsive independent parts [22], and the proposed averaged model represents the averaged behavior of the second part. Moreover, if (12b) does not hold, the algorithm can be easily adapted in order to consider

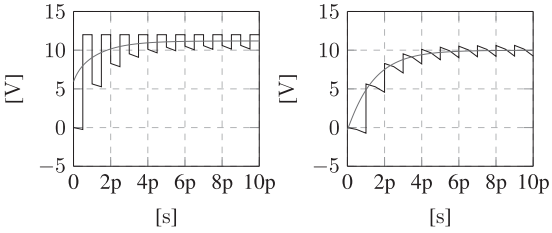

Fig. 6. Time evolutions of the first (left) and second (right) state variables of the ladder converter (see Fig. 2) for $d = 0.5$, $p = 1$ ms, $\alpha = 1000$, $\Delta = 0.003$, $C_1 = C_2 = 12$ μF, $u = 12$ V.

the more general class of inputs representable as the solution of a SDAE.

The matrices V and W are obtained in Algorithm 1 by using the function *getVWspace*. This function exploits the fact that the images of V and W define the consistency space in which the solutions of the differential algebraic equation evolve, say $\mathcal{V}^*$, and its dual space $\mathcal{W}^*$. The spaces $\mathcal{V}^*$ and $\mathcal{W}^*$ can be obtained by considering the so called Wong sequences [9], [23]

$$\mathcal{V}_0 := \mathbb{R}^n,\ \mathcal{V}_{i+1} := A^{-1}(E\mathcal{V}_i),\ i \in \mathbb{N},\ \mathcal{V}^* := \bigcap_{i\in\mathbb{N}} \mathcal{V}_i \quad (44)$$

$$\mathcal{W}_0 := \{0\},\ \mathcal{W}_{i+1} := E^{-1}(A\mathcal{W}_i),\ i \in \mathbb{N},\ \mathcal{W}^* := \bigcap_{i\in\mathbb{N}} \mathcal{W}_i. \quad (45)$$

The function *getVWspace* uses the Wong sequences by implementing Algorithm 2 where the basic MATLAB commands `size`, `eye`, `colspace`, `null`, `rank`, and `zeros` are used.

V. Numerical Results

In this section, we validate the averaged model (40) and (41) through the analysis of numerical results for different SC converters and we propose a design procedure for the jump mode parameter α.

Let us consider the ladder converter shown in Fig. 2. The time evolutions of the states of the switched model (29) with (16) and those of the corresponding averaged model (40) and (41), are reported in Fig. 6. The results show an accurate approximation of the averaged model.

In order to select the parameter α of the jump mode we have considered the error between the solution of the averaged model (40) and (41) and the moving average over the period p of the solution of the switched model, say x_{mv}, which is defined as

$$x_{\text{mv}}(t) = \frac{1}{p}\int_{t-p}^{p} x(\tau)d\tau \quad (46)$$

for $t \in \mathbb{R}_+$, where $x(t)$ is the solution of (29) with $x(\tau) = 0$, for $\tau \in [-p, 0)$. For each simulation over the interval $[0, T]$, we consider the cumulative relative error according to

$$\bar{e} = \frac{100}{T}\int_0^T \frac{\|x_{\text{mv}}(t) - x_{\text{av}}(t)\|}{\|x_{\text{mv}}(t)\|}dt. \quad (47)$$

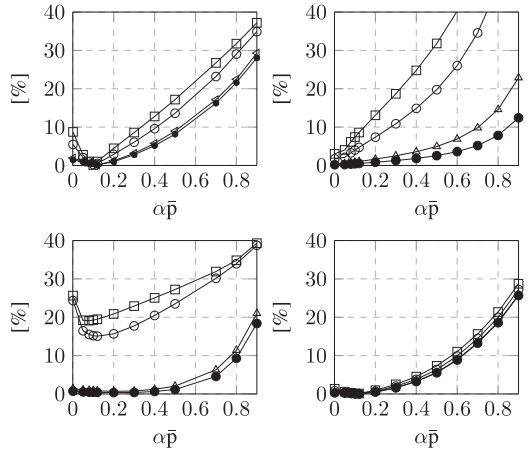

Fig. 7. Error (46) by varying α for the series–parallel converter (see Fig. 3). Each curve is obtained by fixing a specific value of the switching period $\bar{p} \in \{0.2, 0.1, 0.02, 0.01\}$ ms for $\{\square,\ \circ, \triangleleft,\ \bullet\}$, respectively. The parameters and inputs for the nominal (up-left) case are: $C_1 = C_2 = 12$ nF, $C_o = 0.1$ μF, $R = 10$ kΩ with $u = 1.2$ V, $\Delta = 0.003$, and $d = 0.5$. The other figures are obtained by changing the following parameters with respect to the nominal case: $d = 0.3$ (bottom-left), $C_o = 0.01$ μF (up-right), $R = 100$ kΩ (bottom-right).

The value of the parameter α has been selected by analyzing the errors that occur by varying α and the switching period p, which result in $\alpha p = 0.1$.

The influence of the parameter α has been analyzed also by considering the series–parallel SC converter shown in Fig. 3 and the corresponding modes matrices (20). In Fig. 7 are reported the error (47) by varying α and by considering different switching periods, circuit parameters, and duty cycles. The results clearly show that, so as typical for the averaged models, the error decreases by decreasing the switching period. This behavior is also confirmed by decreasing α, although for some particular combinations of the converter parameters an unexpected increase of the error for small values of α is detected. However this effect reduces by increasing the switching frequency. In the following we choose $\alpha p = 0.1$.

This value turns out to provide good results for this converter: Fig. 8 shows the time evolutions of the third state variable by varying the input and the circuits parameters.

The effectiveness of the proposed averaged model is confirmed by the reduction of the error between the averaged and the switched models when the switching period decreases. This is confirmed by the results in Fig. 9 where the state variables of the series–parallel converter for different switching periods are shown.

Similar results are obtained for the other SC converters considered above. For instance, by considering the Dickson circuit shown in Fig. 5, the effectiveness of the averaged model (40) and (41) with (27) is confirmed by the results in Fig. 10.

The proposed averaged model can be used also to reproduce the nominal input–output relationship of SC converters. To this aim let us consider the Fibonacci power converter shown in Fig. 4. By using the switched model (29) with (22) and the corresponding averaged model (40) and (41) we have computed the rms output voltage for different switching frequencies and load resistances. The results in Fig. 11 reproduce the well-known

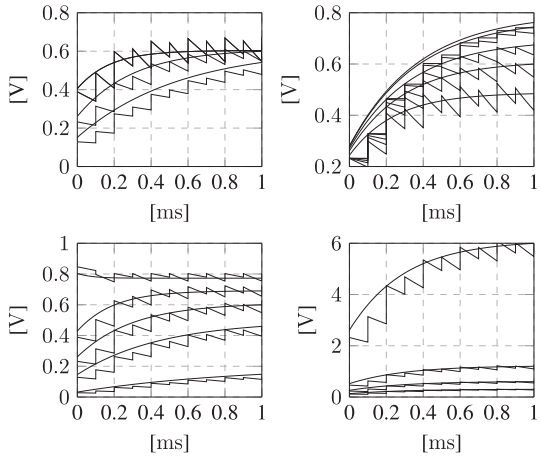

Fig. 8. Time evolutions of the third state variable of the series–parallel converter (see Fig. 3) with $p = 0.2$ ms, $\Delta = 0.003$ and $d = 0.5$. Say $\bar{C}_o = 0.1$ μF, $\bar{R} = 10$ kΩ, $\bar{C} = 12$ nF, $\bar{u} = 1.2$ V. Each figure is obtained by varying a specific parameter/input: (top left) $C_o \in \{0.5\bar{C}_o,\ \bar{C}_o,\ 2\bar{C}_o\}$, $R = \bar{R}$, $C_1 = C_2 = \bar{C}$, $u = \bar{u}$; (top right) $C_o = \bar{C}_o$, $R \in \{0.5\bar{R},\ 1\bar{R},\ 2\bar{R}\ 10\bar{R},\ 100\bar{R}\}$, $C_1 = C_2 = \bar{C}$, $u = \bar{u}$; (bottom left) $C_o = \bar{C}_o, R = \bar{R}, C_1 = C_2 \in \{0.1\bar{C}, 0.5\bar{C},\ \bar{C},\ 2\bar{C},\ 10\bar{C}\}, u = \bar{u}$; (bottom right) $C_o = \bar{C}_o, R = \bar{R}, C_1 = C_2 = \bar{C}, u \in \{0.5\bar{u},\ 1\bar{u},\ 2\bar{u},\ 10\bar{u}\}$.

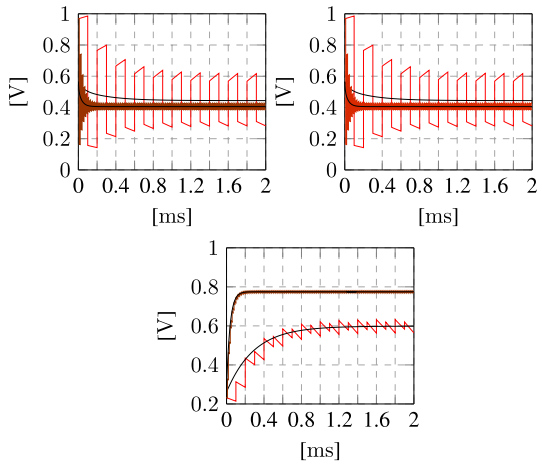

Fig. 9. Time evolutions of the first (top left), second (top right), and third (bottom) state variables of the series–parallel converter (see Fig. 3) for slow switching ($p = 0.2$ ms) and fast switching ($p = 0.02$ ms). The trajectories of the SDAE are colored in red (light for $p = 0.2$ ms, dark for $p = 0.02$ ms), whereas the averaged dynamics are black lines (for $p = 0.2$ ms, and for $p = 0.02$ ms). The circuit parameters/inputs are the same as in Fig. 7.

dependencies [2], [24], with an error that decreases by increasing the switching frequencies.

The dynamic matrix (41) is valid also for non constant duty cycles. In order to show the effectiveness of the averaged model under these operating conditions, we consider duty cycles generated by a pulse width modulation with the sinusoidal modulation signal $0.5 + 0.3\sin(2\pi f_m t)$ where $f_m = f_{\text{sw}}/10$, and a sawtooth carrier signal with switching frequency $f_{\text{sw}} = 1/p$ and unitary amplitude. In Fig. 12, the magnitude of the averaged and switched output voltage spectra for different frequencies are shown. The averaged model spectrum well approximates the frequency behavior of the switched model for low frequencies, moreover, the error decreases by increasing the switching frequency.

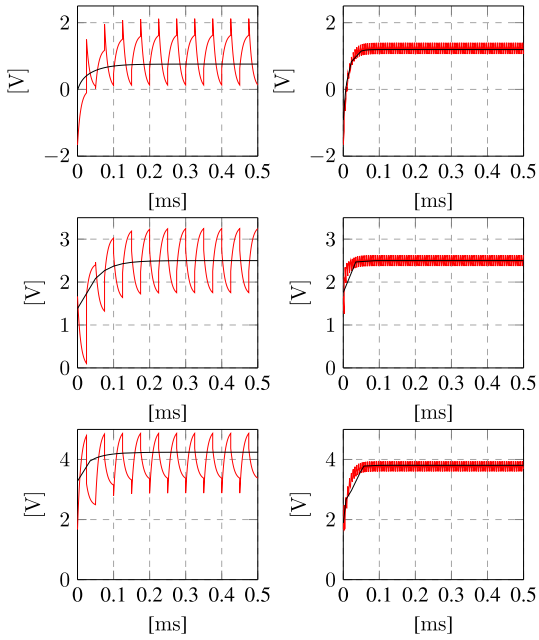

Fig. 10. State variables (first top, third bottom) of the Dickson converter (see Fig. 5) versus time for slow switchings ($p = 0.1$ ms, left) and fast switchings ($p = 0.01$ ms, right). The trajectories of the SDAE are colored in red, whereas the averaged dynamics are black lines. The circuit parameters are $C_1 = C_2 = C_3 = 12$ nF and $R = 1$ kΩ, with $u = 5$ V, $\Delta = 0.003$, and $d = 0.5$.

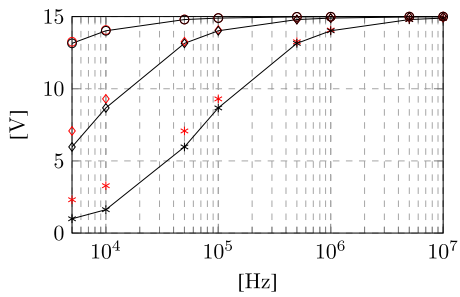

Fig. 11. RMS output voltage of the Fibonacci converter (see Fig. 4) as a function of the switching frequency for different resistances $R \in \{1,\ 10,\ 100\}$ kΩ indicated with $\{*,\ \diamondsuit,\ \circ\}$, respectively. The red and the black data result from the averaged and the switched models, respectively. The circuit parameters are: $C_1 = C_2 = C_3 = 0.1\,\mu$F, $C_o = 0.01\,\mu$F with $u_1 = 3$ V, $u_2 = 0.8$ V, $\Delta = 0.003$, and $d = 0.5$.

The effectiveness of the averaged model is shown also when the constant voltage sources are perturbed with sinusoidal signals. In Fig. 13, the time evolutions of the output voltage of the Fibonacci converter under sinusoidal perturbations on the inputs are shown. Clearly, the averaged variables exhibit a good tracking of the actual averages during transient and in steady state.

VI. Experimental Results

The effectiveness of the switched model (29) and averaged model (40) and (41) has been experimentally verified through specific prototypes built for the series–parallel and Fibonacci converters. The switches are realized by using the ADG451BNZ monolithic CMOS device that includes four independent units with small equivalent resistance and low voltage drop in the ON

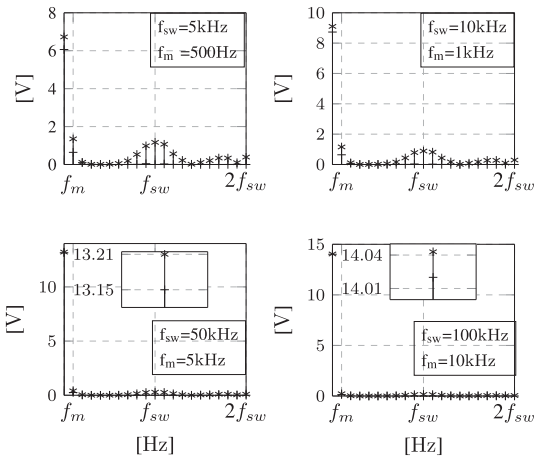

Fig. 12. Magnitude of the output voltage spectrum for the Fibonacci converter (see Fig. 4) with sinusoidal duty cycle and different frequencies. The results of the switched DAE model are $''*''$, whereas the averaged data are $'' + .''$ The circuit parameters and inputs are the same as in Fig. 11 with $R = 10\,\mathrm{k}\Omega$.

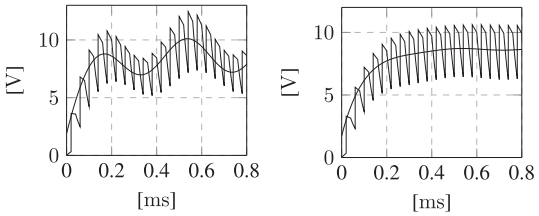

Fig. 13. Time evolutions of the output voltage of the Fibonacci converter (see Fig. 4) with sinusoidal voltage source u_1 (left) and u_2 (right). The circuit parameters are the same as in Fig. 11 with $R = 10\,\mathrm{k}\Omega$; moreover $U = 1$ V, $f_{sw} = 10\,\mathrm{kHz}$ and $\omega = 2\pi\,\mathrm{kHz}$.

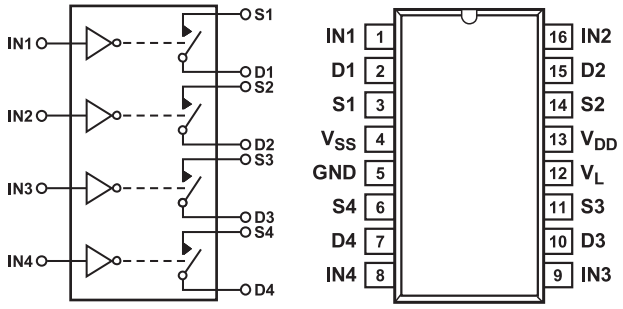

Fig. 14. Functional block diagram (on the left), and PINs configuration (on the right) of the ADG451BNZ device.

state, the switches are turned ON with a logic low on the appropriate control input, see Fig. 14. For the series–parallel converter in Fig. 3 two ADG451BNZ devices are used. The switches $\mathcal{S}_z$ with $z = \{1, 2, 5, 6\}$ are connected to the rest of the circuit through the PINs indicated in Fig. 14 with $(\mathrm{S}_i, \mathrm{D}_i)$, $i = \{1, 2, 3, 4\}$ respectively, and each of them is controlled by the PIN called IN_i, $i = \{1, 2, 3, 4\}$. The switches $\mathcal{S}_z$ with $z = \{3, 4, 7\}$ in Fig. 3 are realized analogously with a second ADG451BNZ. The commands for the control of the switches are determined by a multichannel programmable voltage generator. The PINs indicated with V_L of both group of switches are connected to a 5 V voltage supply, while V_{SS}, V_{DD}, and GND in Fig. 14 are wired up to a programmable voltage supply that provides dc inputs

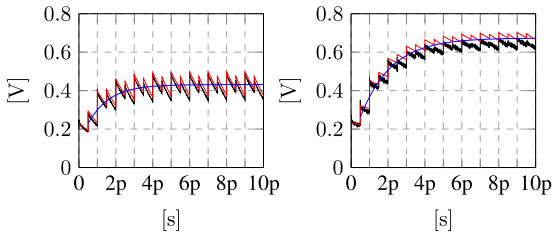

Fig. 15. Time evolutions of the output voltage of the series–parallel converter for $p = 0.5$ ms (left) and $p = 0.1$ ms (right). The circuit parameters/inputs are the same as in Fig. 7. The black lines are experimental data, the red and blue lines are numerical results for the switched and averaged models, respectively.

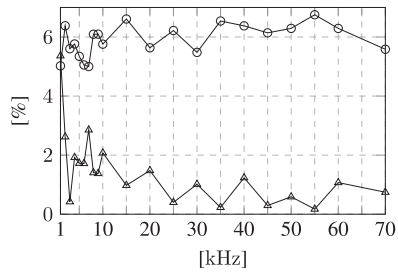

Fig. 16. Steady-state error of the rms output voltage of the series–parallel converter for different switching frequencies: switched model versus experiments ($\circ$), switched model versus averaged model ($\triangle$). The parameters/inputs are the same as in Fig. 7.

of -12, $+12$, and 0 V, respectively. Electrolytic capacitors at the output voltage and ceramic capacitors complete the components required to build the converter. A circuit aided design program has been used to obtain the printed circuit boards from the corresponding netlist.

Let us verify the validity of the SDAE model (29) together with the matrices (20) in order to reproduce the experimental data. In Fig. 15, the time evolutions over the same time interval for two different switching periods are reported. The results confirm the dependence of the steady-state output voltage on the switching frequency and show the effectiveness of the switched and averaged models during transient and in steady-state. As one could argue from the numerical results presented in the previous section, the averaged model (40) and (41) is expected to better approximate the behavior of the real circuit when the switching period decreases. So as shown in Fig. 16, the output voltage of the switched model presents a small steady-state error with respect to the experimental data. The error does not reduce by increasing the switching frequency because of the high frequency effects of the real switches that are not considered in the ideal switches model. This is confirmed by the relative error between the output voltages of the switched and averaged models that is shown in the same figure and it clearly decreases with the frequency. Similar results are obtained for different values of the duty cycle.

Simulations and experiments in time domain are in good agreement also for the Fibonacci converter. The circuit in Fig. 4 has been realized similarly to the series–parallel converter, but with three ADG451BNZ devices. In particular, each device implements and controls correspondingly the following groups of switches $\mathcal{S}_z$: $z = \{1, 5, 8\}$, $z = \{2, 6, 9\}$, and $z = \{3, 4, 7, 10\}$. Fig. 17 shows that the proposed averaged model (40) and (41),

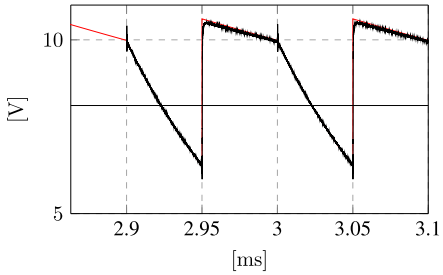

Fig. 17. Steady-state evolution of the output voltage of the Fibonacci converter with $p = 0.1$ ms. The black line are experimental data, the red line are numerical results obtained by considering the SDAE model. The averaged model is a black line. The circuit parameters/inputs are the same as in Fig. 11 with $R = 10\,\mathrm{k}\Omega$.

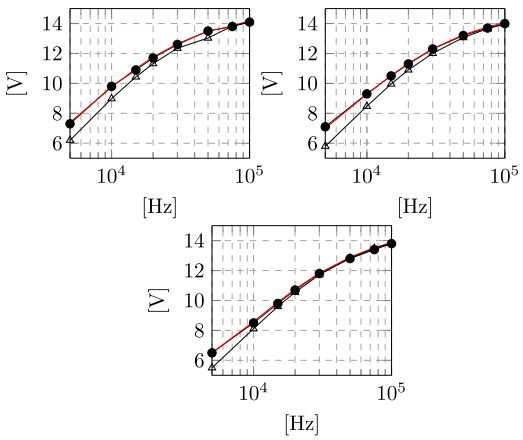

Fig. 18. RMS output voltage of the Fibonacci converter for different duty cycles: $d = 0.25$ (top left), $d = 0.5$ (top right), $d = 0.75$ (bottom) by varying the switching frequency. The other parameters are the same as in Fig. 11 with $R = 10\,\mathrm{k}\Omega$. The black markers ($\bullet$) are experimental data, the red and black markers ($\triangle$) are obtained by numerical simulation, by considering the SDAE and averaged models, respectively.

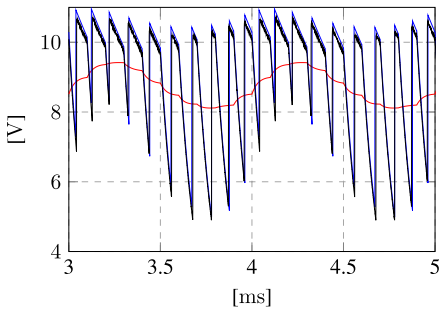

Fig. 19. Time evolution of the output voltage for the Fibonacci converter with $p = 0.1$ ms and sinusoidal modulating signal. The black line are experimental data, the blue and red lines are obtained by simulations, by considering the SDAE and the averaged models, respectively. The circuit parameters/inputs are the same as in Fig. 11 with $R = 10\,\mathrm{k}\Omega$.

obtained from (29) with (22), is able to capture in steady-state the averaged of the output voltage. The good results are confirmed also for different duty cycles and switching frequencies, see Fig. 18. Finally, Fig. 19 shows that for sinusoidal modulating signals the switched model (29) with (26) and the corresponding averaged model (40) and (41) well reproduce the experimental behaviors.

VII. Conclusion

SC converters with ideal switches present discontinuities in the state variables, which complicate the use of the classical switched and averaged models for the analysis of their dynamic behavior. In this paper we have shown how the SDAE framework is effective in order to represent the dynamics of this class of converters without requiring the substitution of the algebraic constraints into the dynamic equations. Then the introduction of jump modes, which approximate the state discontinuities, has allowed the construction of a frequency-dependent averaged model that generalizes the classical one by including the presence of state jumps. The numerical and experimental results obtained by considering ladder, series–parallel, Fibonacci, and Dickson power converters have validated the effectiveness of the proposed switched and averaged models. A direction for future research could be the application of our averaged model for the control design of power converters with state jumps.

Acknowledgment

The authors would like to thank Dr. Stephan Trenn for his comments on SDAE and encouragements on the analysis of the proposed averaged model.

References

[1] S. R. Sanders, E. Alon, H. P. Le, M. D. Seeman, M. John, and V. W. Ng, "The road to fully integrated dc–dc conversion via the switched-capacitor approach," *IEEE Trans. Power Electron.*, vol. 28, no. 9, pp. 4146–4155, Sep. 2013.

[2] M. D. Seeman and S. R. Sanders, "Analysis and optimization of switched-capacitor dc–dc converters," *IEEE Trans. Power Electron.*, vol. 23, no. 2, pp. 841–851, Mar. 2008.

[3] J. C. Mayo Maldonado, J. C. Rosas Caro, and P. Rapisarda, "Modelling approaches for dc-dc converters with switched capacitors," *IEEE Trans. Ind. Electron.*, vol. 62, no. 2, pp. 953–959, Feb. 2015.

[4] L. Müller and J. W. Kimball, "A dynamic model of switched-capacitor power converters," *IEEE Trans. Power Electron.*, vol. 29, no. 4, pp. 1862–1869, Apr. 2014.

[5] T. Souvignet, B. Allard, and X. Lin-Shi , "Sampled-data modeling of switched-capacitor voltage regulator with frequency-modulation control," *IEEE Trans. Circuits Syst. I*, vol. 62, no. 4, pp. 957–966, Apr. 2015.

[6] B. Wu, S. Li, K. M. Smedley, and S. Singer, "Analysis of high-power switched-capacitor converter regulation based on charge-balance transient-calculation method," *IEEE Trans. Power Electron.*, vol. 31, no. 5, pp. 3482–3494, May 2016.

[7] S. Xiong, S.-C. Wong, S.-C. Tan, and C. K. Tse, "Optimal design of complex switched-capacitor converters via energy-flow-path analysis," *IEEE Trans. Power Electron.*, vol. 32, no. 2, pp. 1170–1185, Feb. 2017.

[8] S. Trenn, "Switched differential algebraic equations," in *Dynamics and Control of Switched Electronic Systems—Advanced Perspectives for Modeling, Simulation and Control of Power Converters*, F. Vasca and L. Iannelli, Eds. London, U.K.: Springer-Verlag, 2012, ch. 6, pp. 189–216.

[9] A. D. Domínguez-García and S. Trenn, "Detection of impulsive effects in switched DAEs with application to power electronics reliability analysis," in *Proc. 49th IEEE Conf. Decis. Control*, Atlanta, GA, USA, 2010, pp. 5662–5667.

[10] L. Iannelli, K. Johansson, U. Jönsson, and F. Vasca, "Subtleties in the averaging of a class of hybrid systems with applications to power converters," *Control Eng. Pract.*, vol. 18, no. 8, pp. 961–975, Aug. 2008.

[11] L. Iannelli, C. Pedicini, S. Trenn, and F. Vasca, "On averaging for switched linear differential algebraic equations," in *Proc. 12nd Eur. Control Conf.*, Zürich, Switzerland, 2013, pp. 2163–2168.

[12] L. Iannelli, C. Pedicini, S. Trenn, and F. Vasca, "An averaging result for switched DAEs with multiple modes," in *Proc. 52nd IEEE Conf. Decis. Control*, Florence, Italy, 2013, pp. 1378–1383.

[13] E. Mostacciuolo, S. Trenn, and F. Vasca, "Partial averaging for switched DAEs with two modes," in *Proc. 14th Eur. Control Conf.*, Linz, Austria, 2015, pp. 2901–2906.
[14] E. Mostacciuolo, S. Trenn, and F. Vasca, "Averaging for non-homogeneous switched DAEs," in *Proc. 54th IEEE Conf. Decis. Control*, Osaka, Japan, 2015, pp. 2951–2956.
[15] E. Mostacciuolo and F. Vasca, "Averaged model for power converters with state jumps," in *Proc. 15th Eur. Control Conf.*, Aalborg, Denmark, 2016, pp. 301–306.
[16] S. Trenn, "Distributional differential algebraic equations," Ph.D. dissertation, Institut für Math., , Tech. Univ. Ilmenau, Ilmenau, Germany, 2009. [Online]. Available: http://www.db-thueringen.de/servlets/DocumentServlet?id=13581
[17] O.-Y. Wong, H. Wong, W.-S. Tam, and C.-W. Kok, "Dynamic analysis of two-phase switched-capacitor dc–dc converters," *IEEE Trans. Power Electron.*, vol. 29, no. 1, pp. 302–317, Jan. 2014.
[18] Y. Lei and R. C. N. Pilawa-Podgurski , "A general method for analyzing resonant and soft-charging operation of switched-capacitor converters," *IEEE Trans. Power Electron.*, vol. 30, no. 10, pp. 5650–5664, Oct. 2015.
[19] E. Mostacciuolo, S. Trenn, and F. Vasca, "Averaging for switched daes: Convergence, partial averaging and stability," *Automatica*, vol. 82, pp. 145–157, Aug. 2017.
[20] A. Lopez, R. Diez, G. Perilla, and D. Patino, "Analysis and comparison of three topologies of the ladder multilevel dc/dc converter," *IEEE Trans. Power Electron.*, vol. 27, no. 7, pp. 3119–3127, Jul. 2012.
[21] R. Frasca, M. K. Camlibel, I. C. Goknar, L. Iannelli, and F. Vasca, "Linear passive networks with ideal switches: Consistent initial conditions and state discontinuities," *IEEE Trans. Circuits Syst. I*, vol. 57, no. 12, pp. 3138–3151, Dec. 2010.
[22] S. Trenn and F. Wirth, "Linear switched DAEs: Lyapunov exponent, converse Lyapunov theorem, and Barabanov norm," in *Proc. 51st IEEE Conf. Decis. Control*, Maui, HI, USA, 2012, pp. 2666–2671.
[23] T. Berger, A. Ilchmann, and S. Trenn, "The quasi-Weierstraß form for regular matrix pencils," *Linear Algebra Appl.*, vol. 436, no. 10, pp. 4052–4069, May 2012.
[24] J. M. Henry and J. W. Kimball, "Switched-capacitor converter state model generator," *IEEE Trans. Power Electron.*, vol. 27, no. 5, pp. 2415–2425, May 2012.

Elisa Mostacciuolo was born in Benevento, Italy in 1988. She received the Graduate degree in electronic engineering and the Ph.D. degree in information engineering (with curriculum in automatic control) at the University of Sannio, Benevento, Italy, in 2013 and 2016, respectively.

During the Ph.D. she was visiting student at the University of Kaiserslautern (Germany). She currently has a Post Ph.D. position at the Department of Engineering, University of Sannio. Her research interests include modeling and analysis of switched dynamic systems with applications to power electronics.

Francesco Vasca (SM'XX) was born in Giugliano, Italy, in 1967. He received the Ph.D. degree in automatic control from the University of Napoli Federico II, Naples, Italy, in 1995.

Since 2015, he has been a Full Professor of automatic control in the Department of Engineering, University of Sannio, Benevento, Italy. He was a Visiting Scientist in the Massachusetts Institute of Technology, University of Kaiserslautern and University of Groningen. His research interests include the analysis and control of switched and networked dynamic systems with applications to power electronics, railway control, automotive control, and social networks.

From 2008 to 2014, he has been an Associate Editor for the IEEE TRANSACTIONS ON CONTROL SYSTEMS TECHNOLOGY. Since 2017 he is Associate Editor of Automatica. He served as a Reviewer for several international scientific journals, as a member of the programme committees for many international conferences, and as a member of Ph.D. theses committees at academic institutions in Sweden, France and Spain.

Silvio Baccari was born in Benevento, Italy on May 13, 1975. He received the Graduate degree with honors in computer engineering and the Ph.D. degree in information engineering (with curriculum in automatic control) from the University of Sannio, Benevento, Italy with full marks (*"summa cum laude"*) in 2006 and 2012, respectively.

He was in the Dipartimento d'Ingegneria in the field of remote sensing and automatic control systems. During the Ph.D. degree he has spent the sabbatical period at the Stanford University, Stanford, CA, USA. He is an inventor of some italian patents and author of international scientific papers in the ICT and automatic control areas. He received a Post-Ph.D. position in the Department of Engineering, University of Sannio for the implementation of a "real time" train simulator on a HIL platform. Over the years he increased skills in the field of power electronic devices, microcontrollers, FPGA, and renewable energy sources. He currently designs and implements automatic control systems for an international company in Italy.